J. Min. Metall. Sect. B-Metall. 54 (2) B (2018) 185 - 196

Journal of Mining and Metallurgy, Section B: Metallurgy

EFFECT OF ALLOYING ELEMENTS ON THE STACKING FAULT ENERGIES OF DILUTE AL-BASED ALLOYS

Q. Gao[a], H. Zhang[a], R. Yang[a], Z. Fan[a], Y. Liu[a], J. Wang[b*], X. Geng[a], Y. Gao[a], S. Shang[c], Y. Du[b], Z. Liu[c]

[a] Department of Mathematics and Physics, Chengde Petroleum College, Chengde, China
[b] State Key Lab of Powder Metallurgy, Central South University, Changsha, China
[c] Department of Materials Science and Engineering, Pennsylvania State University, University Park, Pennsylvania, USA

(Received 07 January 2018; accepted 27 April 2018)

Abstract

A systematic study of the stacking fault energy (γ_{SF}) for the dilute Al-based alloys ($Al_{23}X$, $Al_{47}X$ and $Al_{71}X$, where X = Al, Ag, Be, Ca, Cd, Co, Cu, Cr, Fe, Ga, Ge, Hf, In, K, La, Li, Mn, Mg, Ni, Na, Pb, Sc, Sn, Sr, Si, Ti, V, Zn, and Zr) has been performed by means of first-principles calculations. Alias shear deformation is adopted in the present investigations. The presently calculated γ_{SF} for Al is in favorable accordance with experimental and other theoretical data. For the targeted elements, the calculations indicate that Na, Si, K, Ca, Sc, Ga, Ge, Sr, Zr, In, Sn, La, Hf, and Pb, in any concentration we considered, decrease the γ_{SF} of Al, while Ag, Be, Cd, Co, Cu, Cr, Fe, Li, Mn, Mg, Ni, Ti, V, and Zn increase the γ_{SF} of Al, when the concentration of alloying elements is 1.39 at. % in the system. With increasing concentration of alloying elements, Li, Mg, V, Ti, and Cd change from increasing the γ_{SF} of Al to decreasing it, based on present investigations. Among the alloying elements, which decrease the γ_{SF} of Al, La decreases the γ_{SF} most significantly. It is also found that the γ_{SF} of Al-X generally decreases with the increase of equilibrium volume. The results obtained in the present work provide an insight into the design of Al based alloys.

Keywords: *Stacking fault energy; First-principles; Al-based alloys; Alloying element*

1. Introduction

Intrinsic stacking fault is common and important in materials, because it usually can affect the deformation mechanism and mechanical properties of metallic materials，such as plastic deformation, crystal growth, phase transition, strength, and ductility [1-3]. The strength of materials is controlled by the formation and propagation of dislocations, while the ductility or brittleness of a material is related to the strength [4]. It is observed that the kinetic process of partial dislocation movements, such as cross-slip or climb, can be retarded by a lower stacking fault energy (γ_{SF}) [3]. Meanwhile, the steady-state creep rate can be reduced by a lower γ_{SF} [5-7] as well, which is usually expressed approximately as below [8-9],

$$\dot{\varepsilon} \approx \Gamma_{SF}^{n} \tag{1}$$

$$\Gamma_{SF}^{n} = \frac{\gamma_{SF}}{G\mathbf{b}} \tag{2}$$

In Eq. (1), Γ_{SF}^{n} is the normalized stacking fault energy and can be evaluated by Eq. (2), where n is an empirical parameter around 3 to 4 [10]. G and **b** in Eq. (2) are the shear modulus and the Burgers vector, respectively.

In a perfect fcc (face centered cubic) crystal, the stacking sequence of atomic layers along <111> direction is …ABCABC…, where A, B, and C represent nonequivalent three kinds of atomic layers, as shown in Fig. 1. When one atomic layer is removed or glided a distance $a_{fcc}/\sqrt{6}$ along the $<11\bar{2}>$ direction on the {111} layer, the stacking sequence will turn to be ABCABABC…. As a result, an intrinsic stacking fault occurs [11]. Herein, a_{fcc} is the lattice parameter of perfect fcc crystal. γ_{SF} can be calculated by the energy difference between the crystal with a stacking fault and the original perfect crystal, being normalized via the stacking fault area.

Unlike Cu and Ag, the γ_{SF} of Al is large, resulting from the fact that electrons cannot readapt readily in Al due to the directionality of the bonds when intrinsic stacking fault occurs [2]. Many researchers have performed calculations and experiments to deduce the γ_{SF} of Al [12-21]. However, the reported results vary widely, as seen in Table 1. The measured γ_{SF} of Al are 280±50 [15], 135±20 [19], 166 [18], and 150±40 mJm^{-2} [17]. The large uncertainty of these measurements is possibly due to the different methods, experimental conditions, sample purity, the inaccuracies in measuring small differences for the separation distance between partial dislocations [2],

*Corresponding author: wangjionga@gmail.com

DOI:10.2298/JMMB180107007G

and assumptions in the analysis. In the aspect of measuring method, more advanced experimental methods including TEM (transmission electron microscopy) [19] and HRTEM (high-resolution transmission electron microscopy method) [17] must lead to more accurate results than the earlier measured value 280±50 [15]. Computationally, the values of γ_{SF} in Al vary from 95.4 [14] to 162 mJm^{-2} [22]. The difference of 66.6 mJm^{-2} can be regarded as the uncertainty of calculations, which partially comes from the inaccuracies in modeling electronic interactions between atoms using an empirical potential (EP) [23], such as the glue potentials [14] and the phenomenological many-body potentials [24], and partially comes from the models used in the calculations, such as the slab model [22] and the alias shear model [4].

For Al-based alloys, the alloying elements, which include Mg, Ga, Zn, Si, and Cu targeted by Muzyk et al. [22] and Fe, Mn, Cr, Cu, Zn, Mg, Si, Ga, Ti, and Ge by Qi et al. [2] have been investigated through first-principles calculations. In the work of Muzyk et al. [22], the concentration of alloying elements is 2.08% (atomic percent, the same below) in the adopted supercell and 25% at the sliding layer adjacent to stacking fault, while in the work of Qi et al. [2], the concentration of solute atom is as high as 3.3% for the whole system and 33% at the sliding layer adjacent to stacking fault. From Table 1, it can be seen that the results obtained by Muzyk et al. [22] are larger by 20~30 mJ/m^2 than those by Qi et al. [2]. Such a difference may be due to that different mole fractions of alloying elements at the sliding layer adjacent to stacking fault result in different γ_{SF} of Al, which is also verified for Ni based alloys by the recent work of Shang et al. [25]. In addition, in the work of Qi et al. [2] it can be observed that the γ_{SF} values of Al alloyed with Ge and Ti decrease mostly, while the higher γ_{SF} values of Al are from adding Fe and Mn. However, Muzyk et al. [22] reported that alloying elements Fe and Ga lead to higher reduction in the γ_{SF} of Al, while Al alloyed with Mn and Si result in higher γ_{SF}, in which the common alloying element Fe acts on the contrary with that in the work of Qi et al. [2]. In addition, the effects of Mg, Cu, and Zn on the γ_{SF} of Al have been investigated experimentally [26-29]. The reported concentrations of alloying elements in Al from experiments are 0.65% [26], 0.5% [27], 1.1% [27], and 3.25% [27] for Mg, 0.47% [27] and 0.86% [29] for Cu, and 10% [28] for Zn, respectively. For Al alloyed with Mg, the measured values of γ_{SF} decrease with the increasing concentration of Mg. However, the calculated data deviate from the measured ones to some extent, even though the concentrations of Mg are similar. For instance, the data for 3.25% Mg and 3.33% Mg are far away from each other. For Al alloyed with Cu, the values of γ_{SF} decrease with the increasing concentration of Cu, and there exist some divergences between the calculated results and the measured ones. For Al alloyed with Zn, only measured γ_{SF} by Soliman and Mohamed [28] is 150, which agrees well with the result from the work of Muzyk et al. [22], but the concentrations of Zn in the work of Soliman and Mohamed [28] is as high as 10%. As summarized above, there are too many factors, which can affect the accuracy of results. The divergences in the previously reported data and the lacking of systematical study of γ_{SF} for Al-based alloys motivate the present investigation through first-principles calculations. Consequently, the present work aims to investigate the alloying elements (Ag, Be, Ca, Cd, Co, Cu, Cr, Fe, Ga, Ge, Hf, In, K, La, Li, Mn, Mg, Ni, Na, Pb, Sc, Sn, Sr, Si, Ti, V, Zn, and Zr, shown in Table 2), which have been reported as additions in Al alloys [30-31]. More importantly, these results from a systematic study can serve as a guide for future experimental researches as well as computational investigations by using γ_{SF} and corresponding properties.

The remainder of this paper is organized as follows. The method for evaluation of stacking fault energy and the details of first-principles calculations are presented in section 2. The predicted stacking fault energies for Al-based alloys are discussed in section 3. Conclusions obtained in the present work are summarized in section 4.

2. Computational approach

2.1. Prediction of stacking fault energy

Stacking fault energy of an fcc lattice can be evaluated roughly from the energy difference between the hcp and fcc phases [32], or between the hcp, dhcp, and fcc phases [33]. The models to calculate the γ_{SF} have been developed in the literature [11, 34-36]. In the present work, the alias shear deformation is selected to study the stacking fault energies because the numbers of atoms employed in the supercell is only half for a similar study compared to other models [11]. For an alias shear deformation, there exist two kinds of deformation schemes: the simple shear and the pure shear [3-4, 21], in which the simple alias shear scheme uses much less computational resource. More importantly, the value of γ_{SF} from the simple alias shear is similar to the one from the pure alias shear [4]. Hence, the simple alias shear is adopted in the present work to study the effect of alloying elements on the stacking fault energies of Al-based alloys.

$<11\bar{2}>$ direction on the {111} plane is the weak direction for shear deformation in fcc lattice, during which the intrinsic stacking fault occurs [11]. For the sake of simplifying the process for first-principles calculations, an orthorhombic cell containing six

Table 1. *Available experimental and theoretical stacking fault energy (γ_{SF}) of Al and Al alloys, together with the method or models and pseudopotentials used in calculations*

System		γ_{SF}	Method		Year	Ref.
Al	Expt.	280±50	Annealing kinetics of large faulted loops		1965	[15]
	Expt.	135±20	Transmission electron microscopy		1970	[19]
	Expt.	166			1975	[18]
	Expt.	150±40	High-resolution transmission electron microscopy method		1989	[17]
	Calc.	95.4	Force-Matching Method		1994	[14]
	Calc.	122	Green function boundary condition method	PAW-GGA	2008	[13]
		124		US-GGA		
		134		US-LDA		
	Calc.	130	Twin-energy pathways (GPFE) with a dislocation-based mechanistic model, PAW-GGA		2007	[20]
	Calc.	142			1982	[16]
	Calc.	146	Energy difference between fcc and hcp phase		2007	[12]
			PAW-GGA			
	Calc.	158	Alias model		2002	[21]
			US-GGA			
	Calc.	162	Slab model		2011	[22]
			PAW-GGA			
	Calc	101.7	Alias model			PW
		130.8	PAW-GGA			
		131.2				
Al+*x*Cu	0.86%Cu (Expt.)	180	Estimate from creep rate		1988	[29]
	0.47%Cu (Expt.)	190	Mayes electronic creep testing machine		1993	[27]
	2.08%Cu (Calc.)	162.09	Slab model		2011	[22]
			PAW-GGA			
	3.3%Cu (Calc.)	142	Slab model		2007	[2]
			USPP-GGA			
	1.38% (Calc.)	127.8	Alias model			PW
	2.08% (Calc.)	146.6	PAW-GGA			
	4.17% (Calc.)	157.7				
Al+*x*Cr	3.3%Cr (Calc.)	154	Slab model		2007	[2]
			USPP-GGA			
	1.38% (Calc.)	131.9	Alias model			PW
	2.08% (Calc.)	145.7	PAW-GGA			
	4.17% (Calc.)	138.1				
Al+*x*Fe	3.3%Fe (Calc.)	216	Slab model		2007	[2]
			USPP-GGA			
	1.38% (Calc.)	145.4	Alias model			PW
	2.08% (Calc.)	190.2	PAW-GGA			
	4.17% (Calc.)	175				

Table 1 continues on next page

Table 1 continues from the previous page

Al+*x*Ga	2.08%Ga (Calc.)	138.9	Slab model PAW-GGA	2011	[22]
	3.3%Ga (Calc.)	113	Slab model USPP-GGA	2007	[2]
	1.38% (Calc.)	99	Alias model		PW
	2.08% (Calc.)	121.3	PAW-GGA		
	4.17% (Calc.)	112.3			
Al+*x*Ge	3.3%Ge (Calc.)	82	Slab model USPP-GGA	2007	[2]
	1.38% (Calc.)	91.3	Alias model		PW
	2.08% (Calc.)	108.8	PAW-GGA		
	4.17% (Calc.)	93.9			
Al+*x*Mn	3.3%Mn (Calc.)	194	Slab model USPP-GGA	2007	[2]
	1.38% (Calc.)	143.9	Alias model		PW
	2.08% (Calc.)	164.1	PAW-GGA		
	4.17% (Calc.)	175.4			
Al+*x*Mg	0.5%Mg (Expt.)	102	Based on the shear modulus value of aluminum	1993	[27]
	1.1%Mg (Expt.)	87			
	3.25%Mg (Expt.)	54			
	0.65%Mg (Expt.)	90-130	Isothermal annealing of thin foils	1967	[26]
	2.08%Mg (Calc.)	144.75	Slab model PAW-GGA	2011	[22]
	3.3%Mg (Calc.)	118	Slab model NCPP-GGA	2007	[2]
	1.38% (Calc.)	108.1	Alias model		PW
	2.08% (Calc.)	122	PAW-GGA		
	4.17% (Calc.)	123.4			
Al+*x*Si	2.08%Si (Calc.)	139.48	Slab model PAW-GGA	2011	[22]
	3.3%Si (Calc.)	117	Slab model NCPP/USPP-GGA	2007	[2]
	1.38% (Calc.)	94.9	Alias model		PW
	2.08% (Calc.)	115.5	PAW-GGA		
	4.17% (Calc.)	108.9			
Al+*x*Ti	3.3%Ti (Calc.)	104	Slab model USPP-GGA	2007	[2]
	1.38% (Calc.)	103.9	Alias model		PW
	2.08% (Calc.)	94.8	PAW-GGA		
	4.17% (Calc.)	58.6			
Al+*x*Zn	10%Zn (Expt.)	150	Estimate from creep rate	1984	[28]
	2.08%Zn (Calc.)	159.05	Slab model PAW-GGA	2011	[22]
	3.3%Zn (Calc.)	127	Slab model USPP-GGA	2007	[2]
	1.38% (Calc.)	112.4	Alias model		PW
	2.08% (Calc.)	133.8	PAW-GGA		
	4.17% (Calc.)	132.8			

PW = Present work
GGA: Generalized Gradient Approximation
LDA: Local Density Approximation
PAW: Projector Augmented Wave
USPP: Ultrasoft Pseudopotentials
NCPP: Norm-Conserving Pseudopotentials

Table 2. *Alloying elements (X) used in the present work for dilute Al-X alloys, 'pv' or 'sv' after an atomic symbol indicate that the p or s states, respectively, are treated as valence states in first-principles calculations. The second line in unit cell is the atomic radius and the third line is the atom number*

Li_sv	**Be**												
1.54	**1.13**												
3	**4**												
Na_pv	**Mg**											**Al**	**Si**
1.91	**1.6**											**1.43**	**1.34**
11	**12**											**13**	**14**
K_sv	**Ca_pv**	**Sc_sv**	**Ti_pv**	**V_pv**	**Cr_pv**	**Mn_pv**	**Fe**	**Co**	**Ni**	**Cu**	**Zn**	**Ga_d**	**Ge_d**
2.34	**1.97**	**1.64**	**1.45**	**1.35**	**1.27**	**1.32**	**1.27**	**1.26**	**1.24**	**1.28**	**1.39**	**1.4**	**1.4**
19	**20**	**21**	**22**	**23**	**24**	**25**	**26**	**27**	**28**	**29**	**30**	**31**	**32**
	Sr_sv		**Zr_sv**							**Ag**	**Cd**	**In_d**	**Sn_d**
	2.15		**1.6**							**1.44**	**1.57**	**1.66**	**1.58**
	38		**40**							**47**	**48**	**49**	**50**
		La	**Hf_pv**										**Pb_d**
		1.87	**1.59**										**1.75**
		57	**72**										**82**

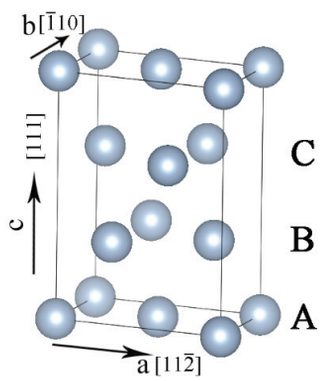

Figure 1. *The geometry of the computational cell used for the investigation of {111} < 11$\bar{2}$ > shear deformations of fcc metals. The three lattice vectors spanning the cell are parallel to the [11$\bar{2}$], [$\bar{1}$10], and [111] directions of the fcc unit cell. Atoms within this cell occupy three closed-packed planes labeled as A, B, and C*

atoms extracted from fcc structure along [111] direction is used in the present work. The lattice vector ***a***, ***b***, and ***c*** of the orthorhombic cell parallel to [11$\bar{2}$], [$\bar{1}$10], and [111] direction of the original fcc lattice, respectively, as shown in Fig. 1. The lengths for ***a***, ***b***, and ***c*** of the orthorhombic cell are $a_{fcc}\sqrt{6}/2$, $a_{fcc}/\sqrt{2}$ and $a_{fcc}\sqrt{3}$ (a_{fcc} is lattice parameter of the fcc cell), respectively. By applying the simple alias deformation along <11$\bar{2}$> direction on {111} plane for fcc lattice, which is along <100> direction on {001} plane in the orthorhombic cell, the lattice vectors R are deformed to $\bar{R}$,

$$\bar{R} = RD \tag{3}$$

$$D = \begin{bmatrix} 1 & 0 & 0 \\ 0 & 1 & 0 \\ \varepsilon & 0 & 1 \end{bmatrix} \tag{4}$$

where R is the initial lattice vector of the orthorhombic cell, D is the deformation matrix, and ε is the engineering shear strain, which is the ratio of displacement after strain ε with respect to the height of the orthorhombic cell.

In the present calculations, three kinds of supercell are employed: 1) a 24-atom (1×2×2) supercell (with respect the 6-atom orthorhombic cell) with 6 {111} layers and 4 atoms in each layer; 2) a 48-atom (2×2×2) supercell with 6 {111} layers and 8 atoms in each layer; and 3) a 72-atom (2×3×2) supercell with 6 {111} layers and 12 atoms in each layer. Alloying element X is placed on the top layer of each supercell, which is the sliding layer adjacent to stacking fault. Correspondingly, the alloy compositions are $Al_{23}X$, $Al_{47}X$ and $Al_{71}X$, respectively. The compositions of X in these three supercells are therefore 1/4, 1/8 and 1/12, respectively, within the sliding layer adjacent to stacking fault. The overall mole fraction y of alloying element X can be derived from the mole fraction within the sliding layer adjacent to stacking fault x,

$$y = x/6 \tag{5}$$

2.2. First-principles calculations details

All first-principles calculations in the present work are based on the density functional theory (DFT), as implemented in the Vienna ab initio simulation package (VASP) code [37]. The projector-augmented-wave (PAW) method [38] is used to describe the electron-ion interaction and the generalized gradient approximation (GGA) by Perdew-Burke-Ernerholf (PBE) [39] is adopted to describe the exchange–correlations functional. The recently recommended electronic configurations of pure elements are employed in the present work, as seen in Table 2. According to the series of tests, a 400 eV cutoff energy, 10×8×3 *k*-points mesh for $Al_{23}X$,

6×10×4 *k*-points mesh for $Al_{47}X$, and 4×5×3 *k*-points mesh for $Al_{71}X$ are enough for energy convergence to less than 1 meV/atom between two ionic steps. For all the calculations in the present work, the Hellman-Feynman force convergence criterion [40] is adopted, based on which the force acts on atoms where they are relaxed to at least -0.01 eV/Å. The Methfessel-Paxton algorithm [41] and the linear tetrahedron method including Blöchl corrections [42] are adopted for structural relaxations and the final energy calculations, respectively. For magnetic elements (Ni, Mn, Fe, Co, and Cr), the spin-polarized approximation is adopted [3].

3. Results and discussions

In this section, we present and discuss the static properties for $Al_{71}X$, $Al_{47}X$, and $Al_{23}X$ at 0 K without considering zero point vibrational energy (ZPE). The targeted properties include the equilibrium volume (section 3.1) and the stacking fault energy (section 3.2).

3.1. Equilibrium volume

Table 3 summarizes the equilibrium volumes (V_0) at 0 K, the relative volumes (ΔV_0^{SF-IS}) for the initial and the stacking fault structures of $Al_{71}X$, $Al_{47}X$, and $Al_{23}X$. It is worth mentioning that the presently predicted V_0 for fcc Al agrees well with the data in the literature [43-48]. For example, the presently computed V_0 of 16.497 Å^3/atom is in excellent agreement with the available theoretical and the experimental value of 16.49 Å^3/atom [43, 46]. As shown in Table 3, in comparison with the initial structures, the structures with stacking fault possess slightly larger volumes with the exception of $Al_{23}Cr$, $Al_{47}Fe$, and $Al_{23}Zr$. Addition of alloying elements usually affect the behavior of charge density redistribution, which may lead to the unusual changes of volumes [3].

To observe the systematic change for V_0 of series of dilute Al alloys, as shown in Table 3, the equilibrium volumes of $Al_{71}X$ are plotted in Fig. 2. It can be observed from Fig. 2 that all of the fourth and the fifth period alloying elements (the fourth and fifth line in Table 2) considered in the present work increase the equilibrium volumes of $Al_{71}X$. However, alloying elements K, Ca, Sc, Ga, and Ge of the third period (the third line in Table 2) can increase the equilibrium volumes of $Al_{71}X$, whereas Ti, V, Cr, Mn, Fe, Co, Ni, Cu and Zn decrease them. For the first and the second period alloying elements (the first and second line in Table 2), Na and Mg increase the equilibrium volumes of $Al_{71}X$ slightly, while Si, Li, and Be act inversely. The biggest increase of equilibrium volume comes from the fourth and fifth period alloying elements. With increasing atomic number of alloying elements in each row, the equilibrium volumes of $Al_{71}X$ decrease firstly and then increase, except for the first and second period alloying elements which are only a few for these two periods. The same tendency of V_0 can be found for $Al_{47}X$ and $Al_{23}X$.

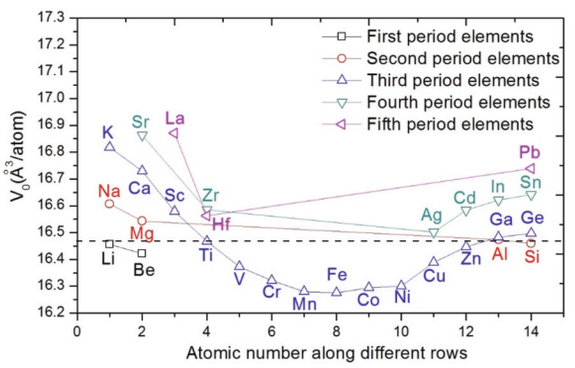

Figure 2. *Predicted equilibrium volume (V_0) for the initial structure of $Al_{71}X$ at 0 K without the effect of zero point vibrational energy. It is plotted as a function of atomic number of alloying element X along different periods, see also table 3*

To facilitate analysis, calculated variation of volume (V) relative to alloying elements (X) for the dilute Al-X alloys is fitted according to the equation below,

$$V(\mathrm{X}) = V_0(\mathrm{Al}) + k_{\mathrm{Vx}}, \tag{6}$$

where k_V is a fitting parameter, and x is the mole fraction of alloying element X. V_0(Al) of 10.497 Å^3/atom is the volume of Al. This value is selected from $Al_{71}Al$, as shown in Table 3, the equilibrium volumes for $Al_{71}X$, $Al_{47}X$ and $Al_{23}X$ are all employed in the linear fittings. The negative value of k_V demonstrates that the equilibrium volume decrease with the increasing concentration of alloying element, while the positive value implies that the alloying element acts the opposite way. From Table 3, it is seen that the largest k_V is caused by alloying element Sr, followed by K and La. Combined with Table 2, it can also be concluded that the radius of alloying element smaller than that of Al usually leads to the positive k_V, while the radius larger than that usually leads to a negative value of k_V, in spite of Ga, Ge, Li, and Ti, whose radius is adjacent to that of Al. The fitted errors, used to reflect the fitting degree between the fitting data and the real values, are also shown in Table 3. For this fitting error, the closer that this value is to 1, the better the linear fitting is. For pure fcc Al, the fitted *k*v should be zero, and the fitting error should be close to 1. The non-zero value of *k*v and the error deviated from 1 indicate the systematic errors of first-principles calculations.

Table 3. *Predicted equilibrium volume for the initial structures of $Al_{71}X$, $Al_{47}X$, and $Al_{23}X$ at 0 K without the effect of zero point vibrational energy, the relative volume for the stacking fault structures with respect to the initial structures (ΔV_{IS0}^{SF-}). Linear fitting parameters for volume (k_V, see equation (10)) due to the effect of alloying element X are also listed, as well as the corresponding fitting errors (err) are also listed. All quantities for volume are in $Å^3$/atom*

	V_0^{IS}	ΔV_{IS0}^{SF-}	V_0^{IS}	ΔV_{IS0}^{SF-}	V_0^{IS}	ΔV_{IS0}^{SF-}		
X	$Al_{71}X$	$Al_{71}X$	$Al_{47}X$	$Al_{47}X$	$Al_{23}X$	$Al_{23}X$	k_V	err
Al	16.4967	0.045	16.4787	0.052	16.4695	0.055	-0.6838	0.737
Ag	16.5189	0.038	16.5168	0.06	16.5433	0.056	0.8774	0.875
Be	16.4181	0.035	16.3124	0.057	16.2903	0.023	-4.6018	0.437
Ca	16.6916	0.051	16.8453	0.045	17.1763	0.028	17.4491	0.991
Cd	16.5558	0.063	16.6401	0.061	16.761	0.064	7.3879	0.955
Co	16.2599	0.072	16.0786	0.149	15.7081	0.141	-18.983	0.992
Cu	16.3597	0.068	16.3548	0.034	16.2089	0.064	-5.4296	0.893
Cr	16.366	0.034	16.328	0.02	16.1486	-0.06	-8.3934	0.991
Fe	16.2896	0.065	16.2332	-0.022	15.9645	0.05	-12.9244	0.986
Ga	16.4995	0.044	16.5017	0.05	16.542	0.04	1.5332	0.703
Ge	16.5067	0.042	16.5254	0.045	16.5784	0.034	2.5806	0.877
Hf	16.5592	0.033	16.6083	0.023	16.709	0.002	5.3918	0.992
In	16.6011	0.054	16.71	0.057	16.8941	0.057	10.5499	0.977
K	16.7717	0.058	16.6832	0.066	17.4608	0.074	24.809	0.807
La	16.8266	0.036	16.7642	0.04	17.6246	0.052	24.1852	0.847
Li	16.4714	0.046	16.4597	0.058	16.4458	0.04	-1.3723	0.548
Mn	16.2918	0.062	16.2323	0.03	16.0424	0.026	-11.5459	0.904
Mg	16.5435	0.047	16.5929	0.055	16.6806	0.044	4.367	0.977
Ni	16.3206	0.063	15.9213	0.113	15.9043	0.196	-16.5535	0.41
Na	16.5936	0.057	16.6747	0.063	16.8459	0.05	9.0802	0.989
Pb	16.7447	0.051	16.8883	0.043	17.2479	0.035	16.7971	0.999
Sc	16.5664	0.039	16.6296	0.03	16.7479	0.01	6.5326	0.985
Sn	16.6169	0.054	16.7407	0.052	16.9645	0.041	12.5144	0.978
Sr	16.8153	0.053	16.7522	0.055	17.6096	0.078	28.5962	0.841
Si	16.4595	0.037	16.4303	0.043	16.4166	0.033	-1.5461	0.378
Ti	16.4799	0.029	16.4523	0.039	16.4534	0.0048	-0.9547	0.152
V	16.4276	0.022	16.3378	0.023	16.3082	0.021	-4.2982	0.567
Zn	16.4623	0.054	16.4494	0.07	16.4085	0.072	2.1764	0.983
Zr	16.5769	0.033	16.6454	0.022	16.7946	-0.006	6.4733	0.986

3.2. Stacking fault energy

Predicted stacking fault energies (γ_{SF}) for $Al_{71}X$, $Al_{47}X$ and $Al_{23}X$ at 0 K are listed in Table 4. The relative stacking fault energy ($^{\triangle}\gamma_{SF}$), which is the energy difference between $Al_{71}X$ and $Al_{71}Al$, $Al_{47}X$ and $Al_{47}Al$, or $Al_{23}X$ and $Al_{23}Al$, are also given in Table 4. The stacking fault energies are estimated at the average volume of the initial structure and the one with stacking fault. The present stacking fault energies predicted using $Al_{23}Al$, $Al_{47}Al$ and $Al_{71}Al$ are 131.2, 130.8 and 101.7 mJm^{-2}, respectively, as shown in Table 4. By comparing with the reliable measured data, 135±20 [19] , 166 [18] , 150±40 mJm^{-2} [17], and the predicted values 120 [49], 122 [13], 124 [13], 134 [13], 130 [20], 142 [16], 146 [12], 158 [21], and 162 mJm^{-2} [22] discussed above, the present results of fcc Al from $Al_{23}Al$ and $Al_{47}Al$ lie in the error range of the reliable experimental data, and also agree well with

most of the theoretical data. The value of $Al_{71}Al$ is a little lower than most of the experimental and theoretical data, which is mainly due to the complexity of Al [2] and the systematic error of the 72-atom supercell which is supported by the previous discussion of V_0 (as shown in Table 3).

Considering the experimental data of Al alloyed with Mg, Cu, and Zn in reference [26-29], it is believable that the concentration of alloying elements impose some extent of impact on the γ_{SF} of Al. The concentrations of Mg, Cu, and Zn in the present study are all different from the ones in available experiments. In addition, there are too many factors that can affect the accuracy of results as described in the introduction section, so there existing some divergences between the results from the present work

Table 4. *The stacking fault energies ($\gamma_{SF,0}$, mJm^{-2}) estimated at the average equilibrium volume of the initial structure and the stacking fault structure (see table 1), together with the available experimental and theoretical data in the literature. The relative stacking fault energies ($\Delta\gamma_{SF,0}$, mJm^{-2}) with respect to those of fcc Al are also shown*

	$\gamma_{SF,0}$	$\Delta\gamma_{SF,0}$	$\gamma_{SF,0}$	$\Delta\gamma_{SF,0}$	$\gamma_{SF,0}$	$\Delta\gamma_{SF,0}$	Calc.	Expt.
X	$Al_{71}X$	$Al_{71}X$	$Al_{47}X$	$Al_{47}X$	$Al_{23}X$	$Al_{23}X$		
Al	101.7	0	130.8	0	131.2	0	95.4[a], 122[b], 124[b], 134[b], 130[c], 142[d], 146[e], 158[f]	280±50[g] 135±20h 150±40i 166j
Ag	119	17.3	138.8	8	146.4	15.2		
Be	117	15.3	149.5	18.7	164.6	33.4		
Ca	79.15	-22.55	70.3	-60.5	65.4	-65.8		
Cd	107.4	5.7	123.3	-7.5	117.2	-14		
Co	149.3	47.6	177.2	46.4	213.8	72.6		
Cu	127.8	26.1	146.6	15.8	157.7	26.5	142[k], 162.09[l]	190[m], 180[n]
Cr	131.9	30.2	145.7	14.9	138.1	6.9	154[k]	
Fe	145.4	43.7	190.2	59.4	175	43.8	216[k]	
Ga	98.97	-2.73	121.3	-9.5	112.3	-18.9	113[k], 138.9[l]	
Ge	91.29	-10.41	108.8	-22	93.85	-37.35	82[k]	
Hf	87.85	-13.85	72.5	-58.3	33.55	-97.65		
In	93.89	-7.81	111.9	-18.9	95.66	-35.54		
K	63.99	-37.71	41	-89.8	-2.6	-133.8		
La	43.54	-58.16	8.1	-122.7	-59.8	-191		
Li	117	15.3	133.9	3.1	128.9	-2.3		
Mn	143.9	42.2	164.1	33.3	175.4	44.2	194[k]	
Mg	108.1	6.4	122	-8.8	123.4	-7.8	118[k], 144.75[l]	90-130[o],102[m], 87[m], 54[m]
Ni	139.3	37.6	163.6	32.8	186.1	54.9		
Na	98.02	-3.68	102.8	-28	79.01	-52.19		
Pb	76.6	-25.1	86.7	-44.1	55.41	-75.79		
Sc	92.58	-9.12	82.6	-48.2	56.56	-74.64		
Sn	81.95	-19.75	98.7	-32.1	73.69	-57.51		
Sr	60.36	-41.34	31.5	-99.3	-14.3	-145.5		
Si	94.87	-6.83	115.5	-15.3	108.9	-22.3	117[k], 139.48[l]	
Ti	103.9	2.2	94.8	-36	58.58	-72.62	104[k]	
V	117.2	15.5	115.7	-15.1	71.71	-59.49		
Zn	112.4	10.7	133.8	3	132.8	1.6	127[k], 159.05[l]	150[p]
Zr	85.19	-16.51	61.6	-69.2	17.21	-114		

Co, Cr, Fe, Mn, Ni are in magnetic situation; a Ercolessi et al. [14]; b Woodward et al. [13]; c Kibey et al. [20]; d Hirth et al. [16]; e Brandl et al. [12]; f Ogata et al. [21]; g Dillamore et al. [15]; h Smallman et al. [19]; i Murr et al. [18]; j Mills et al. [17]; k Qi et al. [2]; l Muzyk et al. [22]; m Soliman et al. [27]; n Chaudhury et al. [29]; o Kritzinger et al. [26]; p Soliman et al. [28]

and the experiments are reasonable. When compared with the previous calculated data by Muzyk et al. [22], the present results with 2.08% X (X = Mg, Ga, Zn, Si, Cu) are 15-25 mJm^{-2} lower. Although we adopted the same content of alloying elements (2.08%) as Muzyk et al. [22] in the present work, different models (alias shear in the present work and slab model in the work of Muzyk et al. [22]) and different content of alloying elements at the sliding layer adjacent to stacking fault (12.5% in the present work and 25% in the work of Muzyk et al. [22]) are adopted. Considering $Al_{23}X$ with the same concentration 25% X at the sliding layer adjacent to stacking fault as that in work of Muzky et al [22], the present predicted results are about 20 mJm^{-2} lower. This is mainly because of the different concentration of alloying elements in the whole system (4.17% in the present work and 2.08% in the work of Muzyk et al. [22]) and the different models. The situation between the present work and Qi et al. [2] is the same as that between the present work and experiments, which is due to the different concentration of alloying elements (1.39%, 2.08%, and 4.17% in the present work and 3.3% in the work of Qi et al. [2] for the whole systems, the corresponding concentrations of alloying elements at the sliding layer adjacent to stacking fault are 8.3%, 12.5%, and 25% in the present work and 33% in the work of Qi et al. [2]) are adopted.

Figure 3 shows the comparisons between the present results of relative stacking fault energy for $Al_{23}X$ with respect to the results evaluated by Muzyk et al. [22]. In both works, the mole fraction of alloying element at the sliding layer adjacent to stacking fault is 25%. Figure 3 shows that the present relative stacking fault energy for $Al_{23}X$ agree well with those from Muzyk et al. [22].

Stacking fault energies of $Al_{71}X$ are illustrated as a function of atomic number of the alloying elements (Fig. 4(a)) and equilibrium volume of $Al_{71}Al$ (Fig. 4(b)). Fig. 4(a) also shows that the alloying elements Na, Si, K, Ca, Sc, Ga, Ge, Sr, Zr, In, Sn, La, Hf, and Pb decrease the γ_{SF} of Al, while the other alloying elements act the opposite way. It is also shown that alloying elements at both ends of each period decrease the stacking fault energy of Al, while the elements in the middle of each period tend to increase it. For all the present alloying elements which decrease the stacking fault energy of Al, the further the element from Al on the periodic table, the larger decrease of the stacking fault energy of Al. Taking the far left alloying elements on each period as an example, the stacking fault energy of Al alloys follows the following trend: $Al_{71}La < Al_{71}Sr < Al_{71}K < Al_{71}Na < Al_{71}Li$. The largest γ_{SF} decreases of Al for the second, the third, the fourth, and the fifth period alloying elements are Si, K, Sr, and La, respectively. Fig. 4(b) shows that the stacking fault energies of $Al_{71}X$

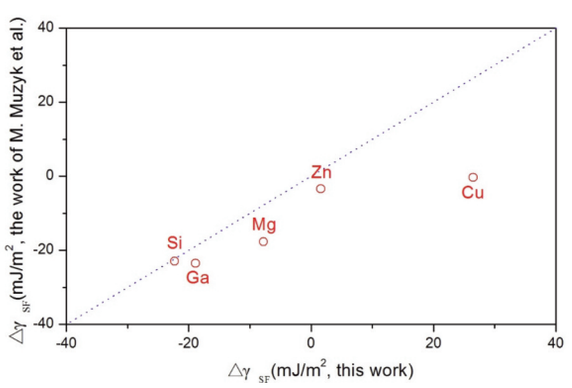

Figure 3. *Comparison of relative stacking fault energy of △ γ_{SF} for Al-X alloys predicted at 0 K. Red ○: this work for $Al_{23}X$ (25% X in stacking fault plane, see table 4) versus first-principles predictions via energy difference between perfect (initial) and faulted structures (25% X in the stacking fault plane) by M. Muzyk et al. [22]. A value of 162.44 mJm^{-2} was predicted for fcc Al by M. Muzyk et al. [22]*

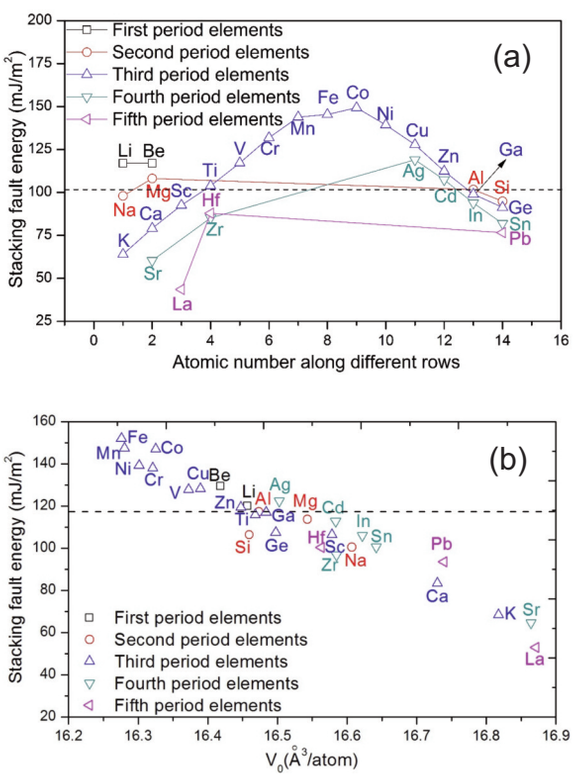

Figure 4. *Stacking fault energy for $Al_{71}X$ at 0 K estimated at the average equilibrium volume of the initial structure and the stacking fault structure (see also table 3 and table 4), displayed as a function of (a). atomic number of alloying element X along different periods; (b). equilibrium volume of $Al_{71}X$*

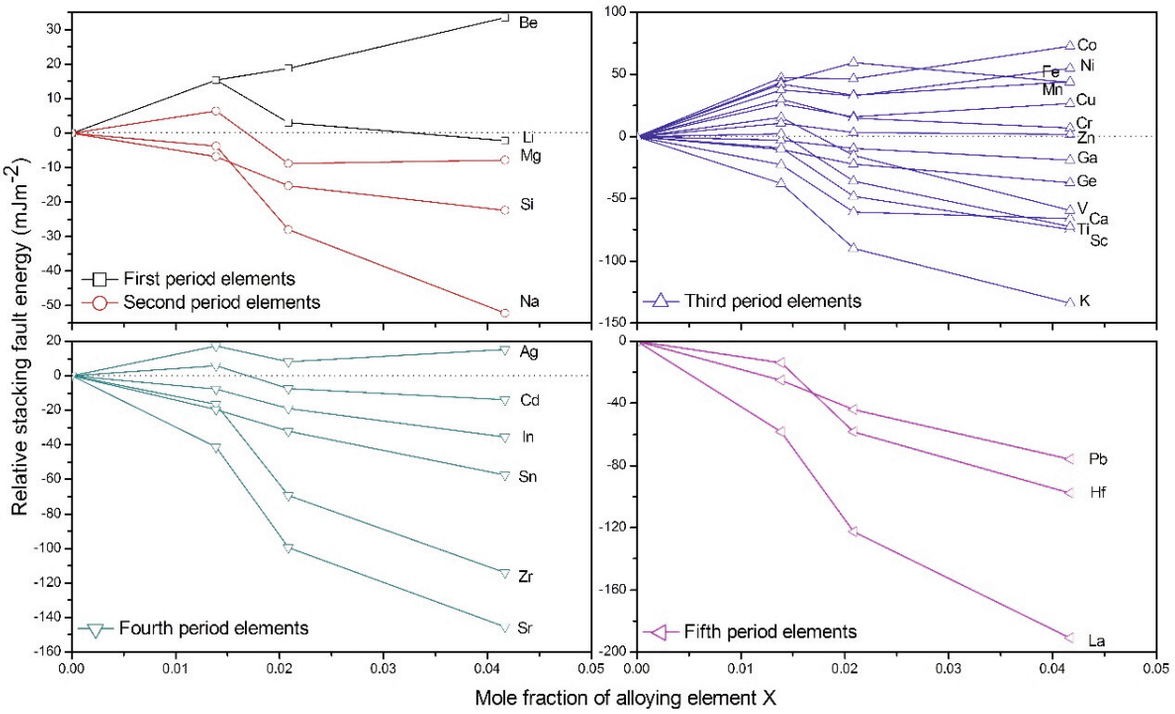

Figure 5. *Relative stacking fault energy for dilute Al-X alloys with respect to Al (101.7, 130.8, and 131.2 mJm^{-2} is adopted here for fcc 72-atoms, 48-atoms and 24-atoms Al, respectively, see table 4) at 0 K, estimated at the average equilibrium volume of the initial structure and the stacking fault structure (see table 3)*

decrease roughly with increasing equilibrium volume of $Al_{71}X$ and all the alloying elements decrease the stacking fault energy of Al from small to large are as follows: La, Sr, K, Pb, Ca, Sn, Zr, Hf, Ge, Sc, In, Si, Na, and Ga. From Fig. 4, it also can be seen that the alloying elements which decrease the stacking fault energy of Al greatly are adjacent to each other, which is similar to the alloying elements which decrease slightly the stacking fault energy of Al. For a better understanding, the relative stacking fault energy values of $Al_{71}X$, $Al_{47}X$, and $Al_{23}X$, as shown in Table 4, are plotted in Fig. 5. From Fig. 5, it is seen that with increasing concentration of alloying element, the effect of Li on the first period, Mg on the second period, V and Ti on the third period, and Cd on the fourth period transfer from increasing the stacking fault energy of Al to decreasing it.

The results of first-principles computations described here verify the dependence of stacking fault energy on the presence of alloying elements. It is found that alloying elements of La, Sr, K, Pb, Ca, Sn, Zr, Hf, Ge, Sc, In, Si, Na, and Ga can reduce the stacking fault energy of Al with 1.39% alloying elements in the whole system. With increasing concentration of alloying elements, Li, Mg, V, Ti, and Cd turn to reduce the stacking fault energy of Al as well. High strength and good ductility are important properties for structural materials. This finding will have an implication for the design of Al alloys, which generally exhibit low ductility due to the lack of efficient strengthening mechanisms.

4. Conclusion

Stacking fault energy for the dilute Al-X alloys ($Al_{71}X$, $Al_{47}X$, and $Al_{23}X$) has been calculated through first-principles calculations in the frame of the alias shear deformation. Twenty-nine alloying elements X (X = Al, Ag, Be, Ca, Cd, Co, Cu, Cr, Fe, Ga, Ge, Hf, In, K, La, Li, Mn, Mg, Ni, Na, Pb, Sc, Sn, Sr, Si, Ti, V, Zn, and Zr) are considered in the present work. The following conclusions are obtained.

Within the considered concentration, alloying elements Na, Si, K, Ca, Sc, Ga, Ge, Sr, Zr, In, Sn, La, Hf, and Pb decrease the stacking fault energy of fcc Al, while the other alloying elements increase it when the concentration of alloying elements is 1.39 at. % in the whole system. With increasing concentration of alloying elements, Li, Mg, V, Ti, and Cd turn to reduce the stacking fault energy of Al.

The alloying elements at both ends of each period (except for the first period which just contains two alloying elements) tend to decrease the stacking fault energy of Al, while the elements in the middle range tend to increase it. For instance, Na and Si at both ends of the second period alloying elements, Ga, Ca,

Sc, Ga, and Ge at both ends of the third period alloying elements, Sr, Zr, In, and Zn at both ends of the fourth period alloying elements, and La, Hf, and Pb at both ends of the fifth period alloying elements decrease the stacking fault energy of Al, while the other elements, such as Mg, Ti, V, Cr, Mn, Fe, Co, Ni, Cu, Zn, Ag, and Cd in the middle part of each period increase it.

For all the alloying elements which decrease the stacking fault energy of fcc Al, the further the element from Al on the periodic table is, the larger decrease of stacking fault energy.

It is also found that the stacking fault energy of Al-X generally decreases with the increase of equilibrium volume.

Acknowledgement

The financial support from the National Natural Science Foundation for Youth of China (Grant No. 51601228, 51429101), the Hunan Provincial Natural Science Foundation for Youth of China (No. 2016JJ3152) and the National Key Research and Development Program of China (Materials Genome Initiative: 2017YFB0701700) are greatly acknowledged. First-principles calculations were carried out partially on the high performance computational clusters provided by the Center of High Performance Computations at Central South University.

References

[1] P.S. Branicio, J.Y. Zhang, D.J. Srolovitz, Phys. Rev. B, 88 (2013) 064104.

[2] Y. Qi, R.K. Mishra, Phys. Rev. B, 75 (2007) 224105.

[3] S.L. Shang, C.L. Zacherl, H.Z. Fang, Y. Wang, Y. Du, Z.K. Liu, J. Phys.: Condens. Matter, 24 (2012) 505403.

[4] M.L. Jahnátek, J. Hafner, M. Krajčí, Phys. Rev. B, 79 (2009) 224103.

[5] A.S. Argon, W.C. Moffatt, Acta Metall., 29 (1981) 293-299.

[6] S. Ma, L. Carroll, T.M. Pollock, Acta Mater. 55 (2007) 5802-5812.

[7] M. Chandranand, S.K. Sondhi, J. Appl. Phys., 109 (2011) 103525.

[8] B. Burton, Acta Metall., 30 (1982) 905-910.

[9] F.A. Mohamed, T.G. Langdon, Acta Metall., 22 (1974) 779-788.

[10] X.S. Xie, G.L. Chen, P.J. McHugh, J.K. Tien, Scr. Metall., 16 (1982) 483-488.

[11] S.L. Shang, W.Y. Wang, Y. Wang, Y. Du, J.X. Zhang, A.D. Patel, Z.K. Liu, J. Phys.: Condens. Matter, 24 (2012) 155402.

[12] C. Brandl, P.M. Derlet, H. Van Swygenhoven, Phys. Rev. B, 76 (2007) 054124.

[13] C. Woodward, D.R. Trinkle, L.G. Hector, D.L. Olmsted, Phys. Rev. Lett., 100 (2008) 045507.

[14] F. Ercolessi, J.B. Adams, Europhys. Lett., 26 (1994) 583-588.

[15] I.L. Dillamore, R.E. Smallman, Philos. Mag., 12 (1965) 191-193.

[16] J.P. Hirth, J. Lothe, Wiley, New York 2nd (1982).

[17] M.J. Mills, P. Stadelmann, Philos. Mag. A 60 (1989) 355-384.

[18] L.E. Murr, Addison Wesley, Reading, MA, (1975).

[19] R.E. Smallman, P.S. Dobson, Metall. Trans., 1 (1970) 2383-2389.

[20] S. Kibey, J.B. Liu, D.D. Johnson, H. Sehitoglu, Acta Mater., 55(2007): 6843–6851.

[21] S. Ogata, J. Li, S. Yip, Science, 298 (2002) 807-811.

[22] M. Muzyk, Z. Pakiela, K.J. Kurzydlowski, Scr. Mater. 64 (2011) 916–918.

[23] J.P. Simon, J. Phys. F: Met. Phys. 9 (1979) 425-430.

[24] A. Aslanides, V. Pontikis, Comput. Mater. Sci., 10 (1998) 401-405.

[25] S.L. Shang, W.Y. Wang, B.C. Zhou, Y. Wang, K.A. Darling, L.J. Kecskes, S.N. Mathaudhu, Z.K. Liu, Acta Mater., 67 (2014) 168-180.

[26] S. Kritzinger, P.S. Dobson, R.E. Smallman, Philos. Mag., 16 (1967) 217-229.

[27] M.S. Soliman, J. Mater. Sci., 28 (1993) 4483-4488.

[28] M.S. Soliman, F.A. Mohamed, Metall. Trans. A, 15 (1984) 1893-1904.

[29] P. Chaudhury, F.A. Mohamed, Mater. Sci. Eng. A, 101 (1988) 13-23.

[30] G.E. Totten, D.S. MacKenzie, Handbook of mechanical alloy design, New York: Marcel Dekker (2003).

[31] V.S. Zolotorevsky, N.A. Belov, M.V. Glazoff, Casting aluminum alloys, Elsevier: Amsterdam (2007).

[32] K. Ishida, Phys. Stat. Sol. A, 36 (1976) 717-728.

[33] L. Vitos, P.A. Korzhavyi, B. Johansson, Phys. Rev. Lett. 96 (2006) 117210.

[34] D.J. Siegel, Appl. Phys. Lett., 87 (2005) 121901.

[35] A. Datta, U.V. Waghmare, U. Ramamurty, Scr. Metar., 60 (2009) 124-127.

[36] J. Han, X.M. Su, Z.H. Jin, Y.T. Zhu, Scr. Meter., 64 (2011) 693-696.

[37] G. Kresse, J. Furthmuller, Phys. Rev. B, 54 (1996) 11169-11186.

[38] G. Kresse, D. Joubert, Phys. Rev. B, 59 (1999) 1758-1775.

[39] J.P. Perdew, Y. Wang, Phys. Rev. B, 45 (1992) 13244-13249.

[40] P.R. Feynman, Phys. Rev., 56 (1939) 340-343.

[41] M. Methfessel, A.T. Paxton, Phys. Rev. B, 40 (1989) 3616-3621.

[42] P.E. Blöchl, O. Jepsen, O.K. Andersen, Phys. Rev. B,

49 (1994) 16223-16233.

[43] Q.N. Gao, J. Wang, S.L. Shang, S.H. Liu, Y. Du, Z.K. Liu, CALPHAD, 47 (2014) 196-210.

[44] J. Wang, S.L. Shang, Y. Wang, Z.G. Mei, Y.F. Liang, Y. Du, Z.K. Liu, CALPHAD, 35 (2011) 562-573.

[45] J. Wang, Y. Du, S.L. Shang, Z.K. Liu, Y.W. Li, J. Min. Metall. Sect. B-Metall., 50 (2014) 37-44.

[46] P. Villars P, L.D. Calvert, Pearson's handbook of crystallographic data for intermetallic phases. ASTM International, Newbury, OH (1991).

[47] S.L. Shang, J. Wang, Y. Wang, Y. Du, Z.K. Liu, Comput. Mater. Sci., 50 (2011) 2096-2103.

[48] J. Wang, Y. Du, X. Tao, Y. Ouyang, L. Zhang, Q. Chen, A. Engstrom, J. Min. Metall. Sect. B-Metall., 53 (2017) 1-7.

[49] R.H. Rautioaho, Phys. Stat. Sol., 112 (1982) 83-89.

UTICAJ LEGIRAJUĆIH ELEMENATA NA ENERGIJU KRISTALNE REŠETKE KOD RAZREĐENIH LEGURA SA OSNOVOM OD ALUMINIJUMA

Q. Gao[a], H. Zhang[a], R. Yang[a], Z. Fan[a], Y. Liu[a], J. Wang[b*], X. Geng[a], Y. Gao[a], S. Shang[c], Y. Du[b], Z. Liu[c]

[a] Odsek za matematiku i fiziku, Fakultet za naftu i gas, Čengde, Kina
[b] Laboratorija za metalurgiju praha, Centralno-južni univerzitet, Čangša, Kina
[c] Odesek za nauku o materijalima i tehniku, Univerzitet u Pensilvaniji, Pensilvanija, SAD

Abstrakt

Sistematično ispitivanje energije kristalne rešetke (γ_{SF}) za razblažene legure sa osnovom od aluminijuma ($Al_{23}X$, $Al_{47}X$ i $Al_{71}X$, gde je X = Al, Ag, Be, Ca, Cd, Co, Cu, Cr, Fe, Ga, Ge, Hf, In, K, La, Li, Mn, Mg, Ni, Na, Pb, Sc, Sn, Sr, Si, Ti, V, Zn, i Zr) izvršeno je uz pomoć jednačina prvog reda. U toku ovog ispitivanja usvojena je defomacija smicanjem. Izračunata γ_{SF} za Al se slaže sa eksperimentalnim i ostalim teorijskim podacima. Za ispitivane elemente, za sve ispitivane koncentracije, proračuni ukazuju da Na, Si, K, Ca, Sc, Ga, Ge, Sr, Zr, In, Sn, La, Hf, i Pb smanjuju γ_{SF} aluminijuma, dok Ag, Be, Cd, Co, Cu, Cr, Fe, Li, Mn, Mg, Ni, Ti, V, i Zn povećavaju γ_{SF} aluminijuma kada je koncentracija legirajućih elemenata u sistemu 1.39 at. %. Na osnovu ovog ispitivanja možemo zaključiti da povećanje koncentracije legirajućih elemenata Li, Mg, V, Ti, i Cd u početku povećava γ_{SF} aluminijuma, a zatim je smanjuje. Među legirajućim elementima koji smanjuju γ_{SF} aluminijuma, La se ističe kao element koji je značajno smanjuje. Takođe se došlo do zaključka da se γ_{SF} legura sa osnovom od aluminijuma uglavnom smanjuje sa povećanjem ravnoteže zapremine. Dobijeni rezultati pružaju uvid u oblikovanje legura sa osnovom od aluminijuma.

Ključne reči: *Energija kristalne rešetke; Jednačine prvog reda; Legure sa osnovom od aluminijuma; Legirajući elementi*